A computer assisted diagnosis system for malignant melanoma using 3D skin surface texture features and artificial neural network

Yi Ding, Lyndon Smith*, Melvyn Smith and Jiuai Sun

Machine Vision Laboratory, Bristol Institute of Technology,
University of the West of England, DuPont Building,
Frenchay Campus, Bristol, BS16 1QY, UK
Fax: +44 (0)117 328 3636
E-mail: Yi3.Ding@uwe.ac.uk
E-mail: Lyndon.Smith@uwe.ac.uk
E-mail: Melvyn.Smith@uwe.ac.uk
E-mail: Jiuai2.Sun@uwe.ac.uk
*Corresponding author

Robert Warr

Department of Plastic Surgery, North Bristol NHS Trust,
Bristol, BS16 1LE, UK
and
Department of Dermatology,
Frenchay Hospital, Bristol, UK
E-mail: robwarr@doctors.org.uk

Abstract: It has been observed that disruptions in skin patterns are larger for malignant melanoma than for benign lesions. In contrast to existing work on 2D skin line patterns, this work proposes a computer assisted diagnosis system for malignant melanoma based on acquiring, analysing and classifying 3D skin surface texture features. Specifically, the 3D skin surface texture, in the form of surface normal vectors are acquired from a six-light photometric stereo device, the 3D features from the surface normals are extracted as the residuals between the acquired data and those from a 2D Gaussian model, while a three-layer feedforward neural classifier is used to classify the residuals. Preliminary studies on a sample set including 12 malignant melanomas and 34 benign lesions have given 91.7% sensitivity and 76.4% specificity using the proposed 3D skin surface normal features, which are better than 91.7% sensitivity and 25.7% specificity using the existing 2D skin line pattern features over the same lesion samples. This demonstrates that the proposed computer assisted diagnosis system of malignant melanoma based on 3D features offers an improvement over that based on 2D skin line patterns.

Keywords: 3D skin texture; a reference skin model; 2D Gaussian function; skin tilt pattern; skin slant pattern; multilayer perceptron; feature enhancement; artificial neural network; ANN; malignant melanoma.

Reference to this paper should be made as follows: Ding, Y., Smith, L., Smith, M., Sun, J. and Warr, R. (xxxx) 'A computer assisted diagnosis system for malignant melanoma using 3D skin surface texture features and artificial neural network', *Int. J. Modelling, Identification and Control*, Vol. X, No. Y, pp.000–000.

Biographical notes: Yi Ding received his Masters from the Centre for Image Communications Research, University of Bristol in March 2005. This degree was about a novel Direct Virtual Viewpoint Synthesis (DVVS) technique used for 3D interactive TV broadcasts. With a strong interest in 3D pattern analysis, simulation and recognition, he is now studying for a PhD on 3D skin surface texture analysis for computer assisted diagnosis of skin cancers at the Machine Vision Laboratory, UWE. He has been working closely with the Pigmented Lesion Clinic at Frenchay Hospital Bristol on the development of a new 3D computer vision based technique to help realise technology for the early diagnosis of skin cancer. His preliminary findings on the analysis of '3D skin surface disruptions' have yielded some promising results, for the differentiation between malignant tumours and benign lesions.

Lyndon Smith is a Reader in Computer Simulation and Machine Vision and Co-director of the Centre for Intelligent Manufacturing and Machine Vision Systems (CIMMS) at UWE. Following his BSc (Hons) in Physics in 1986, he went on to obtain his MSc in Automation in 1988 and PhD

in Computer Simulation of a Manufacturing Process in 1997. In 1998 and 1999 he was the Director of Computer Simulation at a research laboratory at The Pennsylvania State University in the USA. His research activities have resulted in the publication of over eighty technical papers and a book, as well as frequent refereeing of journal papers and the chairing of international research conferences in the USA and Europe.

Melvyn Smith is a Professor of Machine Vision at the Bristol Institute of Technology and Director of the Centre for Intelligent Manufacturing and Machine Vision Systems (CIMMS) at UWE. He received his PhD in 1997, MSc in 1988 and BEng in 1987. He acts as an Associate Editor for four leading international journals, including *Image and Vision Computing* and *Computers in Industry* and is a program committee member for two international conferences. He regularly presents his work through invited seminars, as well as articles and interviews to the popular media. He has been a member of the EPSRC Peer Review College since 2003, served as European commission candidate evaluator for the Sixth Framework and is currently a programme and evaluator/review expert and monitoring expert for EU framework seven programme. He is a Chartered Engineer and an active member of the IET.

Jiuai Sun joined the Machine Vision Laboratory in 2003, where he commenced work on a DPhil which he completed in 2007. His work was based on the fundamental methodology of photometric stereo and its application to skin surface inspection. He also holds a PhD in Biomedical Engineering from Shanghai Jiaotong University, China. His interests are broad and include electronics, optics and computing techniques applicable to healthcare and industry. Currently, his work mainly concerns genuine recovery methods on skin conditions for purposes ranging from dermatology to cosmetics.

Robert Warr is a Consultant Plastic Surgeon at Frenchay Hospital Bristol. He also holds the position of Honorary Senior Lecturer at The University of Bristol and Visiting Senior Research Fellow at UWE. His primary research interest is in the application of novel cutaneous imaging modalities in medicine. His MBBS was gained from Southampton University on 1989. One of his clinical interests is skin cancer and at Frenchay he runs an early diagnostic service for malignant melanoma. In 2001 he was awarded a Doctorate in Medicine from University of Bristol entitled 'The detection of minimal residual disease in malignant melanoma using biological and molecular markers'.

1 Introduction

Malignant melanoma (MM) is one of the most aggressive and life-threatening skin cancers. During the last 30 years, the incidence rates of MM have increased more than any other cancers in the UK. Successful treatment of this dermatological disease relies heavily on early discovery and diagnosis. Realisations of a non-invasive, automated diagnostic aid could offer a useful approach for early differentiation between melanoma and benign pigmented lesions. Conventionally, a group of 2D skin heuristics called the asymmetry, border, colour and diameter (ABCD) rules have been used as the inputs to a lesion classification system. However, the diagnosis accuracy has not been convincing (Sboner et al., 2003). To improve the existing diagnosis, new parameters which can provide additional indications on the presence of MM are needed.

It is known that human skin is covered by a fine network of skin texture patterns. Motivated by the observation that skin texture patterns tend to be disrupted by MM but not by benign lesions, a new texture-based method, namely skin line pattern has been found complementary to the ABCD rules (She et al., 2007). By estimating skin line pattern disruptions from 2D skin lesion images, this method is able to differentiate between MMs and benign lesions. However, the skin line patterns extracted from 2D images can only be considered as pseudo profiles of skin surface, since a 2D image is insufficient to describe a 3D object completely. Additionally, the 2D images are subject to sidelight effects and prone to specularities and shadows.

It is difficult to capture 3D topography data of the skin due to the dynamic, variegated and multilayered characteristics of the skin. Therefore carrying out explicit 3D skin texture analysis for computer assisted diagnosis of MM is still at an early stage. Previous work (Sun et al., 2007) has proposed a six-light source photometric stereo device that provides a detailed and comprehensive description of the skin surface. It can obtain both accurate surface reflectance and surface normals independent from external environmental effects such as ambient illumination. Preliminary evidence suggests that the information obtained should be more suitable than conventional photographs for the purposes of visual and automated assessment of skin (Sun et al., 2008; Ding et al., 2007, 2008a, 2008b).

In contrast to previous work on 2D skin line pattern, this work explores whether analysis of skin surface normal data can yield useful indicators, in the form of 3D skin surface disruptions, for computer assisted diagnosis of MM. Specifically, the surface normal vectors will be analysed through their tilt and slant directions, so called skin tilt pattern and skin slant pattern. In order to detect the subtle skin surface pattern disruptions, a variable 3D skin model is needed to equalise variable 3D topographies of lesions and in other words, the 3D skin model should be able to match

correspondingly for both flat and elevated (or non-flat) lesions' topographies by adjusting its parameters while at the same time detecting its skin slant pattern disruptions. A natural candidate that can meet those demands for a skin slant pattern model would be a 2D Gaussian function.

With the availability of high-speed computing powers, artificial neural networks (ANN), in the last two decades, have been employed extensively as pattern classifiers in medical diagnosis. The paper then evaluates their performance for lesion classification using a feedforward backpropagation neural network. Being insensitive to the variations in the quality of input data and capable of selecting pertinent features for a diagnosis problem (Karunakar and Datta, 2008), make ANN a preferred method over other expert systems (Ercal et al., 1994). Recent evidence has shown that the combination of statistical models with ANN has proved to be very successful for finding system abnormality in the residuals (Chetouani, 2008).

The steps in the proposed approach can be summarised as:

1 Recover surface normals using the six-light photometric stereo device (known as skin analyser).

2 Fit a 2D Gaussian function to the lesion by optimising its parameters.

3 Extract the skin tilt (slant) pattern model from this Gaussian function.

4 Use the residuals between the skin tilt (slant) pattern model and the acquired tilt (slant) pattern to quantify the 3D skin surface disruptions.

5 Classify lesions to either malignant or benign based on the estimated 3D skin surface disruptions using an ANN classifier.

The classification results from the proposed computer assisted diagnosis system based on 3D skin surface normal features will be compared with those based on the existing 2D skin line pattern features.

2 Foundations of the data acquisition system

2.1 The theory of photometric stereo

The surface normal vectors used for the analysis in the current study are acquired from a six-light photometric stereo system known as skin analyser; its theoretical foundations are briefly outlined here. For an ideal Lambertian surface, the image irradiance equation can be expressed as:

$$i = \rho \frac{-p\cos\alpha\sin\beta - q\sin\alpha\sin\beta + \cos\beta}{\sqrt{p^2+q^2+1}} \tag{1}$$

where α and β are slant and tilt angles of the illuminates, the partial derivatives p = dz/dx and q= dz/dy are the x-axis component and y-axis component of the surface gradients respectively and ρ is the surface reflection rate (albedo). Although the surface height z can be reconstructed through the combination of p and q, this process is subject to a number of limitations and can introduce errors, so our approach will be focused on analysing the surface normals directly. From equation (1), we have:

$$i = \rho(\cos\alpha\sin\beta, \sin\alpha\sin\beta, \cos\beta)\cdot\frac{(-p,-q,1)^T}{\sqrt{p^2+q^2+1}} \tag{2}$$

where T denotes the transpose. According to Horn (1986):

$$\overrightarrow{N} = (n_x, n_y, n_z) = \frac{(-p,-q,1)}{\sqrt{1+p^2+q^2}} \tag{3}$$

where $\overrightarrow{N}$ is the surface normal vector. n_x, n_y and n_z are its components in the x-axis, y-axis and z-axis respectively. Hence, the surface gradient vectors can also be calculated as:

$$p = -\frac{n_x}{n_z} \text{ and } q = -\frac{n_y}{n_z} \tag{4}$$

Substituting equation (3) into equation (2), we have:

$$i = \rho\cdot(\cos\alpha\sin\beta, \sin\alpha\sin\beta, \cos\beta)\cdot(n_x, n_y, n_z)^T \tag{5}$$

Since a unit surface normal has a modulus of 1, only three variables are unknown, including the albedo and any two from n_x, n_y and n_z. So we need at least three lights to solve the equation. All other lights offer redundant information which can be used for detecting problematic pixels subject to specularities and shadows allowing them to be removed them from the computation of the skin surface normal and reflectance images (Sun et al., 2007). Since surface normals reflect inherent geometrical properties of 3D surface(s), they are also referred as topographic texture or 3D surface texture (Smith et al., 2000).

2.2 Skin tilt pattern and skin slant pattern

Figure 1 depicts the data acquisition system which is a six-light photometric stereo device known as the skin analyser on the left. One of the six sample lesion images captured by the system is shown in the middle and the recovered surface normals are shown on the right. When used in clinical trials, it is placed with its axis perpendicular to the skin surface and a camera takes six images with each under a different LED illumination. The entire operation takes less than one second, so it meets the demand of the static setup required by photometric stereo. Figure 2 shows that every surface normal on the surface can be identified by its tilt direction ϕ and slant direction θ, which can also be represented by surface gradients as:

Figure 1 Left: the skin analyser (six-light photometric stereo) in operation; middle: one of six skin lesion images taken by the skin analyser, right: recovered surface normal map of the lesion (see online version for colours)

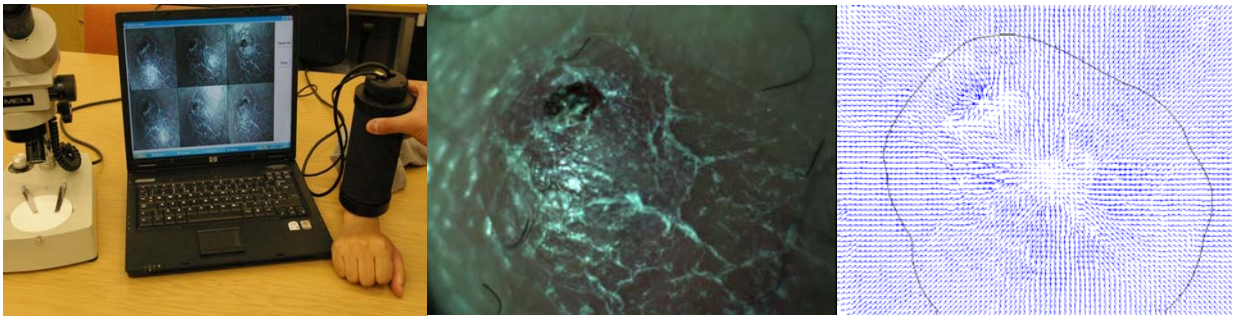

Figure 2 A surface normal vector (n_x, n_y, n_z): its tilt direction is ϕ and its slant direction is θ

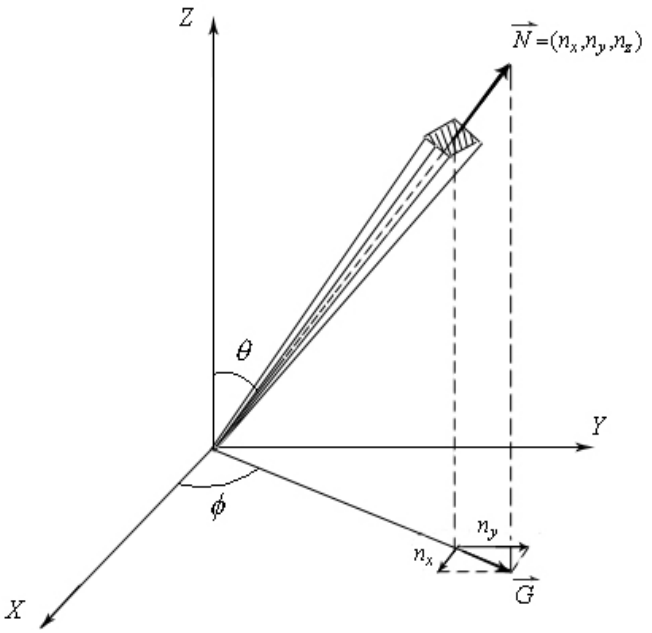

$$\phi = \begin{cases} \tan^{-1}\left(\frac{n_y}{n_x}\right) = \tan^{-1}\left(\frac{q}{p}\right) & \text{if } n_x \geq 0 \text{ AND } n_y \geq 0 \\ 2\pi + \tan^{-1}\left(\frac{n_y}{n_x}\right) = 2\pi + \tan^{-1}\left(\frac{q}{p}\right) & \text{if } n_x \geq 0 \text{ AND } n_y \leq 0 \\ \pi + \tan^{-1}\left(\frac{n_y}{n_x}\right) = \pi + \tan^{-1}\left(\frac{q}{p}\right) & \text{otherwise} \end{cases} \quad (6)$$

$$\theta = \cos^{-1}(n_z) = \cos^{-1}\left(\frac{1}{\sqrt{(p^2+q^2)+1}}\right) \quad (7)$$

where $\vec{G}$ in Figure 2 is the projected vector of the surface normal vector $\vec{N}$ on the image plane. It can be observed that equation (6) is made up of the surface gradient direction and equation (7) is related to the surface gradient magnitude. The employment of the normal tilt angle ϕ and slant angle θ will give more instinctive physical meanings than that of surface gradient or normal. Also, analysing those two quantities is an alternative and more efficient way of analysing the surface normals. Therefore, the surface normal components in the tilt and slant direction may be referred to as the 'skin tilt pattern' and the 'skin slant pattern'.

3 Feature extraction and enhancement

3.1 A variable 3D skin model

Having obtained the surface normal vectors for each lesion, the next step is to estimate their respective skin disruptions. In order to achieve this, a reference skin model is established, whose surface normals can be used as a reference to be compared with the actual surface normals of the lesion.

Depending on the lesion's location on the body, the skin topography can differ from a near flat shape to a slightly raised shape. If a reference skin model is chosen with a flat topography, the amount of surface disruption can be measured directly by calculating the surface normal differences between a lesion and the reference skin in the slant and tilt directions. This approach is feasible for measuring flat lesions but not for raised lesions with a cross section tended to a hemisphere. For spherical lesions, the underlying surface topography will influence the surface normal distributions. As a result of this, previously used surface normal patterns for textured skin are no longer valid. Figure 3 illustrates this by using a texture composed of regular triangles where the textured skin pattern appears as isosceles, with a disrupted skin pattern shown as a dotted scalene on the left. On the right of the figure, the dotted hemisphere represents a hemispherical shaped lesion, on which the skin texture pattern is regularly distanced and well maintained. Here the surface normal vector $\overline{N_{bs}}$ from the hemispherical lesion has the same direction as the one $\overline{N_{ds}}$ from the disrupted flat skin pattern. If both are compared with the surface normal $\overline{N_s}$ from the reference skin model, they will yield the same directional difference. This means that if both are presented to the skin model, they will be recognised as the same surface normal and have the same degree of directional disruption. However, this clearly is not the case, as one is from an area of benign skin and the other is from an area of malignant skin.

Figure 3 Surface normal from a patch of disrupted skin is shown as $\overrightarrow{N_{bs}}$, benign textured skin is shown as $\overrightarrow{N_s}$ and also benign textured skin on a raised spherical lesion is shown as $\overrightarrow{N_{bs}}$.

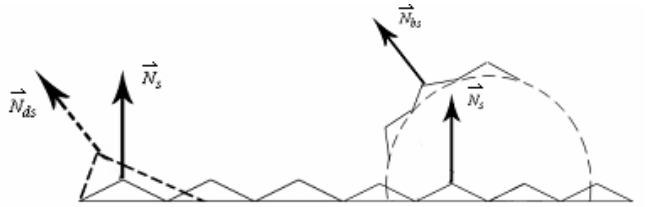

To tackle this problem, this work proposes to use a variable 3D skin model to analyse the 3D skin surface pattern disruptions. The purpose of employing such a 3D variable skin model is to adaptively select a 3D skin model that best fits a lesion's obtained skin surface patterns from skin analyser. A natural candidate in this category would be a 2D Gaussian function. Reasons for this can be explained as follows.

- Firstly, it is the most frequent distribution in real life and is widely used in various parametric statistical hypotheses and analyses. It is envisaged that anything abnormal such as MM are likely to exhibit large deviations from those normal statistics.
- Secondly, its flexibility and variability allows it to approximate a wide range of 3D topographies include topographies with sharp protrusions where the variances are set small and the amplitude large, near flat topographies where the variances are large and the amplitude low, and hemispherical topographies where only the central part of the Gaussian envelope is used. Therefore it is a 3D model that is required for 3D analysis and is fundamentally different from conventional 2D analysis of ABCD features and skin line patterns.
- Thirdly, a Gaussian distribution has a symmetrical contour, therefore it allows for asymmetry analysis of the 3D data.
- Fourthly, the changes in surface gradients between adjacent pixels on a Gaussian envelope are smooth. Therefore the similarity between neighbouring surface gradients is high, which is useful to simulate the regular skin slant patterns which also have large correlations among neighbours.

3.2 Disruptions in skin tilt pattern

The shape of a Gaussian distribution may be denoted as:

$$Z^*(u,v) = A^* \, \mathrm{e}^{-\frac{(u-u_c^*)^2+(v-v_c^*)^2}{2\sigma^2}} \tag{8}$$

As shown in equation (6), the skin tilt pattern is a direction defined entirely within the lesion area on the x-y image plane, so it can be used to determine the centre location of a Gaussian distribution. The star sign '*' denotes an estimated variable.

Figure 4 The skin tilt pattern at a point (u, v) can be determined by its distance to the distribution centre (u_c*,v_c*) in x-axis and y-axis, hence it can be calculated as $\phi^* = \tan^{-1}\left(\|v - v_c^*\| / \|u - u_c^*\|\right)$ where ||.|| denotes the Euclidean distance

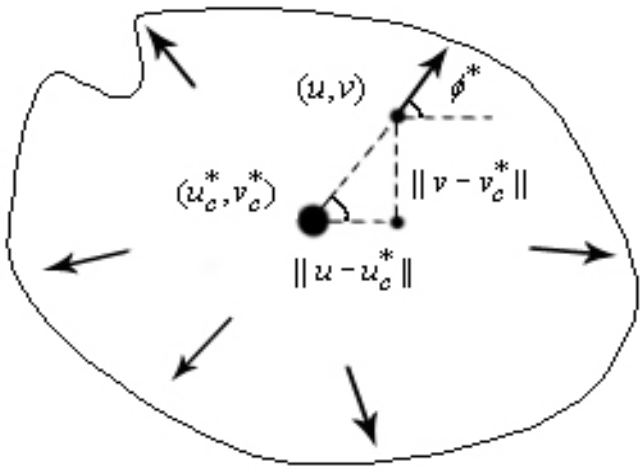

Suppose a 2D Gaussian envelope has a centre of (m_c^*, n_c^*) with equal variance in the x-axis and y-axis. By projecting the Gaussian envelope onto the image plane, we obtain an isotropic distribution of tilt directions centred at (m_c^*, n_c^*). Regarding an isotropic distribution, as shown by Figure 4, the tilt direction for every point (m, n) of the isotropic distribution can be determined by its distance to the distribution centre (m_c^*, n_c^*) in the x-axis and y-axis. Hence, by specifying the centre of the Gaussian function, we can effectively generate a map of the tilt directions for every point in the image. Since the centre of Gaussian function can be anywhere on the image, we can generate a series of Gaussian envelopes whose number depends on the number of points within the image. In relation to the skin reference model, the aim is to find a surface description that is closest to a lesion, so the centre of the Gaussian function have to be the one whose Gaussian function best fits (or more formally, giving the minimum directional differences) a lesion's existing surface normal distribution from the skin analyser. This can be described by the following equation (Ding et al, 2008a).

$$(u_c^*, v_c^*) = \arg\min \sum_{\{(u,v)\} \in S_l} \| (\phi(u,v) - \phi^*(u,v)) \| \tag{9}$$

where (m_c*, n_c*) is the estimated centre of the Gaussian function using minimum error estimation (or least square estimation), S_l denotes the lesion region, ||.|| denotes the Euclidean distance, ϕ is the acquired tilt direction and ϕ^* is the tilt pattern of the Gaussian function.

As shown in Figure 5, given a lesion's acquired skin tilt patterns on the left (marked as 'lesion'), a set of different simulated 'pseudonormal' skin tilt pattern models are

generated by specifying their respective distribution centres, (u_c^1, v_c^1) ,..., (u_c^{N-1}, v_c^{N-1}), (u_c^N, v_c^N) where N is the number of pixels within the lesion region. Among them, only the simulated pseudo normal skin tilt pattern model, (marked as 'skin') which best-fits (i.e., having the smallest differences to) a lesion's acquired skin tilt patterns is chosen for estimating the skin tilt pattern disruptions.

Figure 5 The best-fit skin tilt pattern model (labelled as the 'skin') is estimated as the one having the minimum differences to the lesion's acquired skin tilt patterns (labelled as the 'lesion') among all the skin tilt models generated by the isotropic distributions identified by their respective distribution centre, $\{(u_c^1, v_c^1), \ldots, (u_c^{N-1}, v_c^{N-1}), (u_c^N, v_c^N)\}$

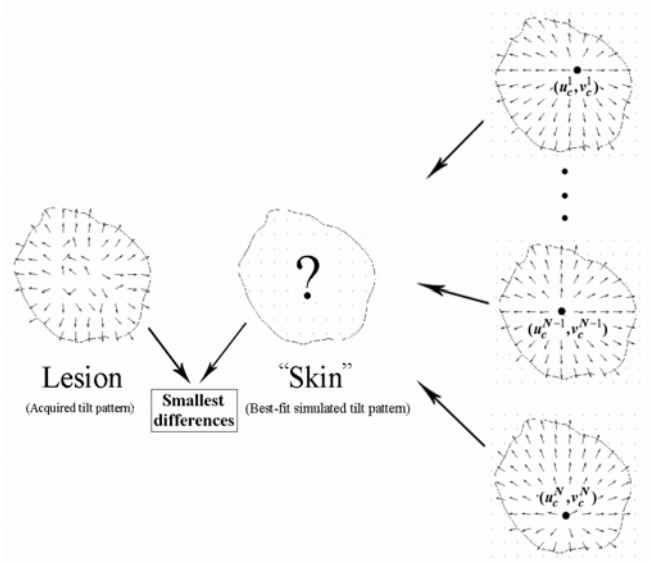

Upon finding this distribution centre, the associated directional differences are defined as the Overall disruptions in skin tilt pattern (OT) between the skin tilt patterns $\phi^*_{\min}$ of the best fit Gaussian function and the existing skin tilt patterns ϕ.

$$\overline{\phi_\Delta} = \frac{\sum_{(u,v)\in S_l} \| (\phi^*_{\min}(u,v) - \phi(u,v)) \|}{S_l} \tag{10}$$

3.3 Disruptions in skin slant pattern

So far, for finding the centre location of the Gaussian distribution, all the computations are limited to the x-y plane and the tilt direction. To determine the exact topography of the Gaussian distribution, the slant directions should also be used.

Since the topography of a Gaussian distribution is dependent on it variance and amplitude, by varying the variance and the amplitude, different Gaussian distributions with different topographies are generated. Among them, only the topography or portions of the topography that gives the minimum differences in skin slant pattern to a lesion's existing skin slant patterns is used to quantify the surface disruptions. This can be defined by the following equation (Ding et al., 2008a)

$$(A^*, \sigma^*) = \arg\min \sum_{(u,v)\in S_l} \left\| \theta^*(u,v) - \theta(u,v) \right\| \tag{11}$$

where

$$\theta = \cos^{-1}(n_z) = \cos^{-1}\left(\frac{1}{\sqrt{p^2+q^2+1}}\right)$$

and

$$\theta^* = \cos^{-1}(n_z^*) = \cos^{-1}\left(\frac{1}{\sqrt{(Z_x^*)^2+(Z_y^*)^2+1}}\right)$$

(Z_x^*, Z_y^*) are the surface gradients in the x-axis and y-axis of the Gaussian functions, S_l denotes the lesion region, ||.|| denotes the Euclidean distance, and σ^* specifies the Gaussian envelope's variance (which is equal in both x-axis and y-axis), while p and q are the obtained surface gradients of a lesion from the skin analyser.

The process of estimating the disruptions in skin slant pattern can also be explained in Figure 6. In this Figure, the acquired skin slant patterns of a nodular lesion are illustrated on the left (marked 'lesion'). In order to estimated the disruptions in skin slant pattern, the acquired skin slant patterns need to be compared with a series of simulated pseudo-normal skin slant patterns (i.e., surface gradients) extracted from a series of different 3D Gaussian topographies (based on 2D Gaussian functions) with variable amplitudes A, variances in the x-axis and y-axis (σ_x, σ_y) and the rotation angle τ, identified by $\{(A^1, \sigma_x^1, \sigma_y^1, \tau^1), \ldots, (A^{n-1}, \sigma_x^{n-1}, \sigma_y^{n-1}, \tau^{n-1}), (A^n, \sigma_x^n, \sigma_y^n, \tau^n)\}$.

Upon determination of σ^* and the resultant Gaussian topography or portions of the Gaussian topography, the associated differences are used to define the degree of disruptions in skin slant pattern. Because there is a trigonometric relation between the modular of surface gradients and the slant direction according to equation (7), the Overall disruptions in skin slant pattern (OS) is defined as the sum of the directional differences between the skin slant patterns $\theta^*_{\min}$ of the best fit Gaussian function and the existing skin slant patterns θ.

$$\overline{\theta_\Delta} = \frac{\sum_{(u,v)\in S_l} \left\| \theta^*_{\min}(u,v) - \theta(u,v) \right\|}{S_l} \tag{12}$$

Figure 6 Among all the skin slant pattern models generated by the 2D Gaussian functions identified by their respective amplitude A, variance in the x-axis, σ_x, variance in the y-axis σ_y and rotation angle τ, i.e., $\{(A^1,\sigma_x^1,\sigma_y^1,\tau^1),\ldots,(A^{n-1},\sigma_x^{n-1},\sigma_y^{n-1},\tau^{n-1}),(A^n,\sigma_x^n,\sigma_y^n,\tau^n)\}$, the best fit simulated pseudonormal skin slant pattern model (labelled as the 'skin') is estimated as the one having the minimum differences to a lesion's acquired skin slant patterns (labelled as the 'lesion')

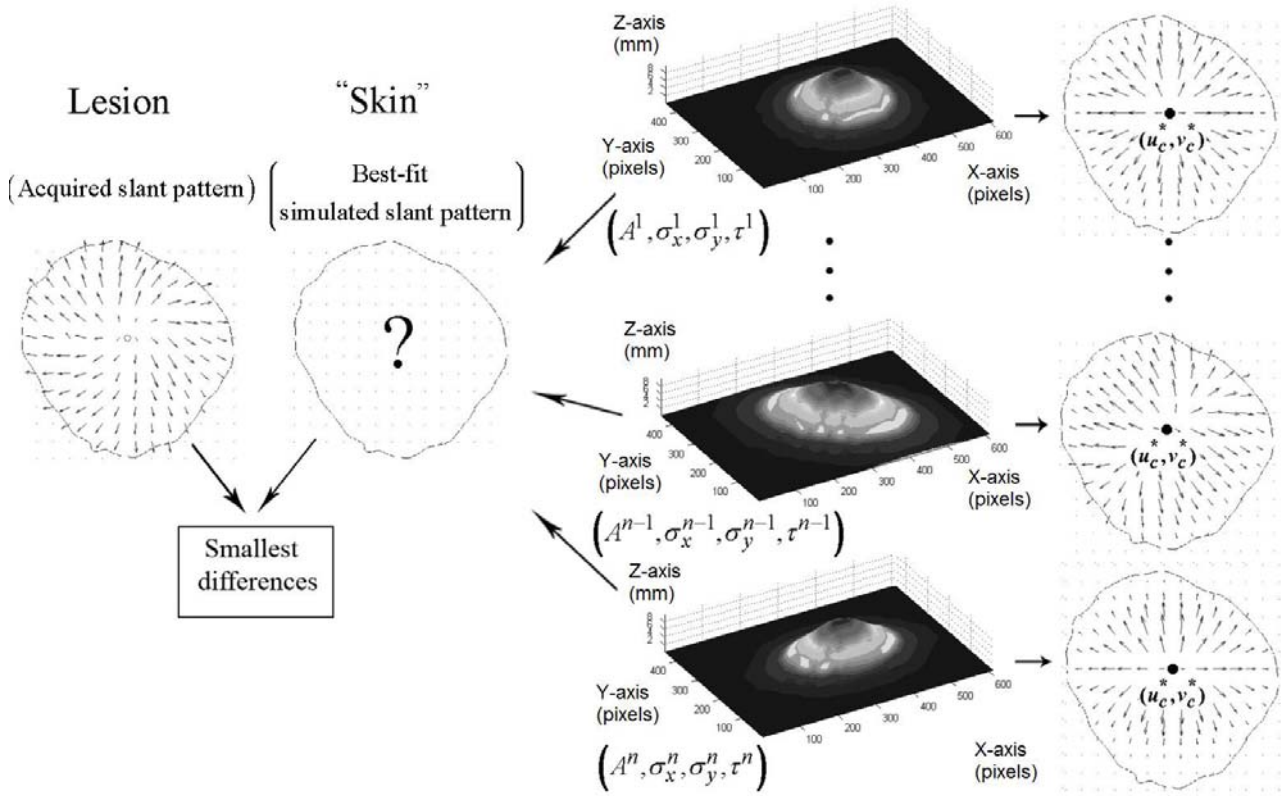

Notes: It should be noted that only magnitudes of surface gradients are related to skin slant patterns as derived in equation (7).

3.4 Feature enhancement

A post-processing filtering step (Ding et al., 2008b) is proposed to enhance both the tilt and slant pattern disruptions by reducing the noise level. Conventional linear filters, e.g., a low pass filter, can remove large amount of noise, but regions of interest are deemed to be noise and filtered as well. Instead, non-linear filtering which can remove high-frequency noise from data is suitable for the task. As one of the most promising nonlinear filtering techniques in recent years, anisotropic nonlinear diffusion is applied here.

The structure tensor J is used to represent the local structure of the skin tilt/slant pattern disruption ε [(i.e., $\overline{\phi_\Delta}$ in equation (10) and $\overline{\theta_\Delta}$ in equation (12)] at each pixel,

$$J(\nabla\varepsilon)=\nabla\varepsilon\cdot\nabla\varepsilon^T=\begin{bmatrix}\nabla\varepsilon_x^2 & \nabla\varepsilon_x\nabla\varepsilon_y\\ \nabla\varepsilon_x\nabla\varepsilon_y & \nabla\varepsilon_y^2\end{bmatrix} \tag{13}$$

where $\nabla\varepsilon_x$ and $\nabla\varepsilon_y$ denote the x-axis and y-axis gradient of the skin tilt/slant pattern disruption. Through eigendecomposition, the local structure tensor can be represented as:

$$J(\nabla\varepsilon)=\begin{bmatrix}\mathbf{v}_1 & \mathbf{v}_2\end{bmatrix}\cdot\begin{bmatrix}\lambda_1 & 0\\ 0 & \lambda_2\end{bmatrix}\cdot\begin{bmatrix}\mathbf{v}_1 & \mathbf{v}_2\end{bmatrix}^T \tag{14}$$

where λ_1, λ_2 (with $\lambda_1 \geq \lambda_2$) are the eigenvalues correspond to the eigenvectors $\mathbf{v}_1$, $\mathbf{v}_2$. The eigenvector $\mathbf{v}_1$ is the direction of the maximum gradient variation locally, i.e., a local feature, thus the smoothing strength should be small along this direction.

A diffusion equation is then used to smooth out the noise within the local skin tilt/slant pattern disruption at each pixel.

$$\varepsilon_t=\mathrm{div}(\mathbf{D}\cdot\nabla\varepsilon)=\mathrm{div}\left(\begin{bmatrix}D_{11} & D_{12}\\ D_{21} & D_{22}\end{bmatrix}\cdot\begin{bmatrix}\nabla\varepsilon_x\\ \nabla\varepsilon_y\end{bmatrix}\right) \tag{15}$$

where ε_t denote the derivative of ε over time t, div(.) is the divergence operator, i.e.,

$$\mathrm{div}(f)=\frac{\partial f_x}{\partial x}+\frac{\partial f_y}{\partial y} \tag{16}$$

D is the diffusion tensor, which controls the smoothing strength, and is defined as a function of the structure tensor, i.e.,

$$\mathbf{D} = \begin{bmatrix} \mathbf{v}_1 & \mathbf{v}_2 \end{bmatrix} \cdot \begin{bmatrix} e^{-\frac{|\nabla \varepsilon|}{T}} & 0 \\ 0 & 1 \end{bmatrix} \cdot \begin{bmatrix} \mathbf{v}_1 & \mathbf{v}_2 \end{bmatrix}^T = \begin{bmatrix} D_{11} & D_{12} \\ D_{21} & D_{22} \end{bmatrix} \quad (17)$$

where $|\nabla \varepsilon|$ is the magnitude of the local gradient in skin tilt/slant pattern disruption, the parameter T is used as a threshold to judge whether local structure is a feature or not, and is chosen empirically.

Thus using the Euler forward difference approximation, the diffusion equation of equation (15) becomes

$$\begin{aligned} \varepsilon^{(t+1)} = \varepsilon^{(t)} + \tau(&\frac{\partial}{\partial x}(D_{11}\varepsilon_x^{(t)}) + \frac{\partial}{\partial x}(D_{12}\varepsilon_y^{(t)}) \\ &+ \frac{\partial}{\partial y}(D_{21}\varepsilon_x^{(t)}) + \frac{\partial}{\partial y}(D_{22}\varepsilon_y^{(t)})) \end{aligned} \quad (18)$$

According to Weickert (1998), the iteration step τ should be chosen as a value smaller than $0.5/N_d$ where N_d is the number of signal dimensions.

4 Classification experiments and results

4.1 Experimental setup

Experiments are carried out on 46 lesions, of which 12 are MMs and nine other types of benign lesions. The 34 benign lesions include four dermatofibromas, five intradermal nevi, three hyperkeratotic squamous papillomas, eight compound nevi, eight seborrhoeic keratoses, two dysplastic nevi, two congenital nevi, one junctional nevus and one blue nevus. All of these lesions were captured at the collaborating institutes using the skin analyser.

However, since the size of the MM samples is reasonably small and the number of benign lesions is more than double the number of MMs, training of the artificial neural network will bias towards a better decision boundary for the benign lesions but a poorer one for the MMs. Artificial neural network theory and practice suggests that, in a diagnostic application, the network should be trained with a balanced mixture of inputs from each diagnostic class (Freeman and Skapura, 1991). However, some lesion classes in the current experiment have only a small number of samples (including blue nevus, junctional nevus, congenital nevus and hyperkeratotic squamous papilloma).

To compensate for this disadvantage in prior probability, the samples for the benign lesions are split into four similar sized groups, which are tested separately against the same 12 MMs as shown in Table 1. Specifically, sample Group 1 includes: one junctional nevus and eight compound nevi based on the fact that both lesions are typically small, smooth and slightly raised. Sample Group 2 includes: eight seborrhoeic keratoses which are among the most common classes of benign lesions and have a distinct appearance from other benign lesions, sample Group 3 includes: five intradermal nevi and four dermatofibroma based on the fact that they both have raised and nodular shape. Sample group 4 is made up of the rest of the benign lesions including two dysplastic nevi, two congenital nevi, three hyperkeratotic squamous papilloma and one blue nevus.

4.2 A three-layer feedforward neural classifier

ANN are mathematical models inspired by the structure of natural neurons, the power and complexity of neural networks as well as the adaptive learning mechanisms in the human brain. They can be applied to function approximation, solution of optimisation problems, simulation of biological processes as well as to pattern recognition problems.

4.2.1 Input

Two features are used as inputs to the three-layer feedforward neural network, i.e., the overall disruption in skin tilt pattern [or OT in equation (10)] and the overall disruption in skin slant pattern [or OS in equation (12)]. To tackle the false 'disruptions' caused by noise, the skin tilt pattern and skin slant pattern disruptions are both enhanced by 30 iterations of anisotropic nonlinear diffusion (equation (18)] with an iteration step of 0.1 and the threshold K of 0.4 for the tilt pattern and an iteration step of 0.1 and K of 2 for the slant pattern. The number of iterations is chosen empirically as it gives a classification result with a reasonable computational cost. Therefore the two features used for lesion classification will be the OT and the OS based on the enhanced skin tilt pattern disruption and skin slant pattern disruption respectively.

4.2.2 Choice of architecture

A three-layer multilayer perceptron (MLP) neural network with backpropagation training is used for classification. Two inputs are the overall disruption in skin tilt pattern and the overall disruption in skin slant pattern. Samples for each input are normalised to zero mean and unit standard deviation (Bishop, 1995). The classifier outputs one indicating MM and zero otherwise. Two hidden layers use sigmoid activation functions while the output layer is linear. According to (Duda et al., 2001), the number of hidden neurons should be chosen as $n/10$, where n is the number of lesion samples. In our case, there are 20 samples so the number of hidden neurons would be two. However, it is envisaged that MLP with only two neurons will have very limited function approximation capability, so slightly more neurons are employed in the current experiment. The exact number of neurons for each layer is determined through the corresponding classification performances, of which the configuration of (2, 2, 1) for the 1st, 2nd and output layer performs best while having the least complexity.

Table 1 Benign lesions are split into four sample groups with benign lesion classes

Sample group	*Lesion class*	*Number in class*	*Total*
Group 1	Compound nevus	8	9
	Junctional nevus	1	
Group 2	Seborrheic keratosis	8	8
Group 3	Intradermal nevus	5	9
	Dermatofibroma	4	
Group 4	Hyperkeratotic squamous papilloma	3	8
	Congenital nevus	2	
	Dysplastic nevus	2	
	Blue nevus	1	

4.2.3 Training

The MLP for each sample group is trained using 'variable learning rate' gradient descent algorithm. While the least mean squared error is used as the cost function between the training output and the target output. Random initialisation of the MLP's neuron weights is required to avoid being trapped in a local minimum during the network training. Although one key advantage of neural networks over linear classifiers is that it can model arbitrary complex decision boundaries, excessive training in a three-layer neural network with many weights can lead to poor generalisation as the net implements an over complex decision boundary 'tuned' to the specific training data rather than the general properties of the underlying distributions. This is a general phenomenon referred as 'overfitting' (Duda et al., 2001). To avoid this, network training should be stopped before the gradient descent completes. One solution is to stop training when the cost error on a separate validation set reaches a minimum. In the current experiment, because the sample Group 1 and the sample Group 3 all have 21 samples, while the sample Group 2 and the sample Group 4 all have 20 samples. So while sample Group 1 (or sample Group 2) is used as the training set, sample Group 3 (or sample Group 4) can be used as the validation set and vice versa.

4.2.4 Testing

Leave-one-out cross validation (LOOCV), a non-biased procedure for testing small sample sets, is used to generalise the MLP's classification performance. This is done by leaving one sample for testing and the remaining samples for training each time. The same procedure is repeated for the next sample and finished until all the samples are tested once. The overall classification rates are calculated as the average successful rate for all the samples.

4.3 Experimental results

The classification performance is compared with the 2D skin line pattern features (She et al, 2007) including the skin line direction (SLD) and the skin line variation (SLV) over the same sample set using the same neural classifier. The feature scatter plots for the two techniques over all samples are shown in Figure 7. Figure 8 lists the classification results using a 3-layer MLP classifier based on the proposed 3D skin surface normal features, (OT and OS) and the 2D skin line pattern features, (SLD and SLV) respectively.

It can be seen from Figure 8 that although both the 2D skin line pattern features and the proposed 3D skin surface normal features demonstrate the same result in sensitivity (the percentage of successful MM classification), the 2D skin line pattern features consistently show a much poorer performance in specificity (the percentage of successful benign lesion classification) across all sample groups. The difference in classification performance is the biggest for the group 1 of include junctional and compound nevi while it is the smallest for the group 3 of seborrhoeic keratoses. Overall, the 3D skin surface normal features achieve a promising classification result of 91.7% sensitivity and 76.4% specificity, which is substantially better than the 2D skin line pattern features, which only achieve a classification result of 91.7% sensitivity and 25.7% specificity.

Figure 7 (a) scatter plot of all lesion samples using the SLD and SLV (b) scatter plot of all lesion samples using the proposed OT and OS (see online version for colours)

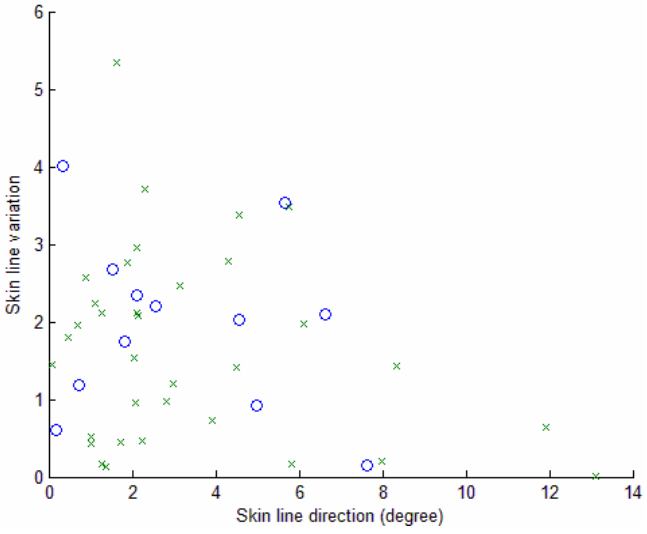

(a)

Figure 7 (a) scatter plot of all lesion samples using the SLD and SLV (b) scatter plot of all lesion samples using the proposed OT and OS (continued) (see online version for colours)

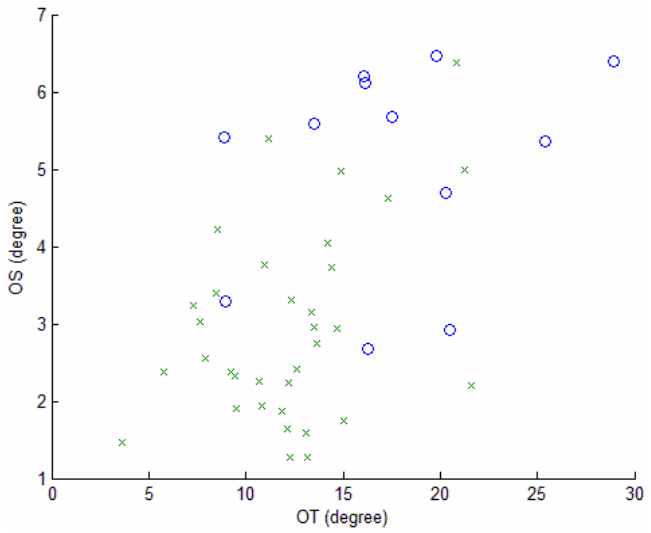

(b)

Figure 8 Classification performances using a three-layer MLP classifier based on: (a) the 3D skin surface normal features (OT and OS), (b) the 2D skin line pattern features (SLD and SLV) (see online version for colours)

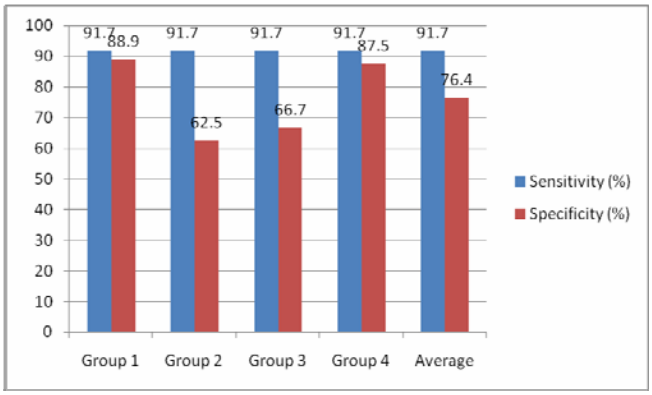

(a)

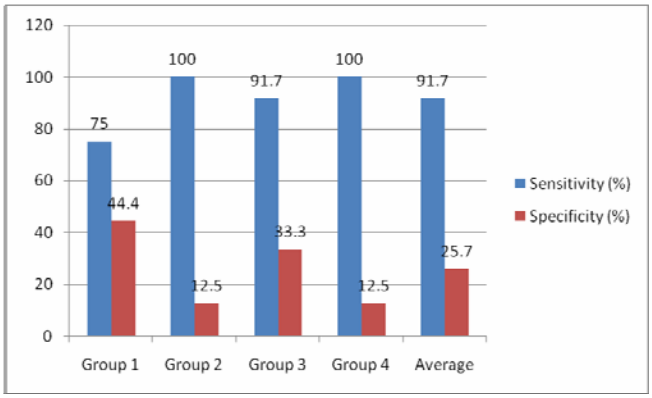

(b)

It appears that the Group 2 which includes seborrhoeic keratoses and the Group 3 which includes intradermal nevi and dermatofibromas have the least classification rates for both techniques. Since both techniques are concerned about the disruptions in skin texture patterns, this agreement in finding is likely to suggest that certain lesions in the two sample groups also have large degree of surface disruptions which prevent them from being classified as benign lesions. Still the classification performance based on the proposed 3D skin surface normal technique demonstrates a much better performance than that based on the 2D skin line pattern technique.

It is noted that the proposed skin surface normal features show a reasonably good classification performance for the Group 4 which includes two classes of 'difficult' benign lesions, i.e., dysplastic nevus and congenital nevus. Lesions from those two classes used in the experiments were even misclassified by the experienced dermatologists at the collaborating clinics, and all have subsequently been sent for biopsies. Dysplastic nevus in particularly has generally been acknowledged as one of the most difficult lesions to be classified by human expert as this class of benign lesions bear large resemblances with MM in terms of surface characteristics. Therefore, a good classification by the proposed features indicates that they may be able to provide the dermatologists with complementary information in addition to the existing ABCD features that would help improve the accuracy of the clinical diagnosis. A substantial improvement in classification performance over the 2D skin line pattern features is also observed in this group.

Receiver-operating-characteristic (ROC) curves are used to evaluate the individual discriminating capability of the four features including the SLD, the SLV, the OT and the OS over all lesion samples. The benign lesions are treated as one benign lesion class rather than with respect to each individual benign lesion class. The ROC curves of all lesion samples for the four features are shown in Figure 9. The ROC areas of all benign lesion samples versus the 12 MM for the OT and OS are 0.87 and 0.78 respectively, both are better than 0.59 and 0.56 achieved by the SLD and the SLV. Among the four features, OS shows the best ROC result. This is probably because the skin slant pattern is defined in the Z-axis direction, which can reveal extra dimensional information. In comparison, SLD is inherently a 2D feature, while the skin tilt pattern is defined on the 2D x-y plane and can only reveal the topographic variations in the plane.

Figure 9 Receiver-operating-characteristic curves: (a) SLD, (b) SLV, (c) OT and (d) OS (see online version for colours)

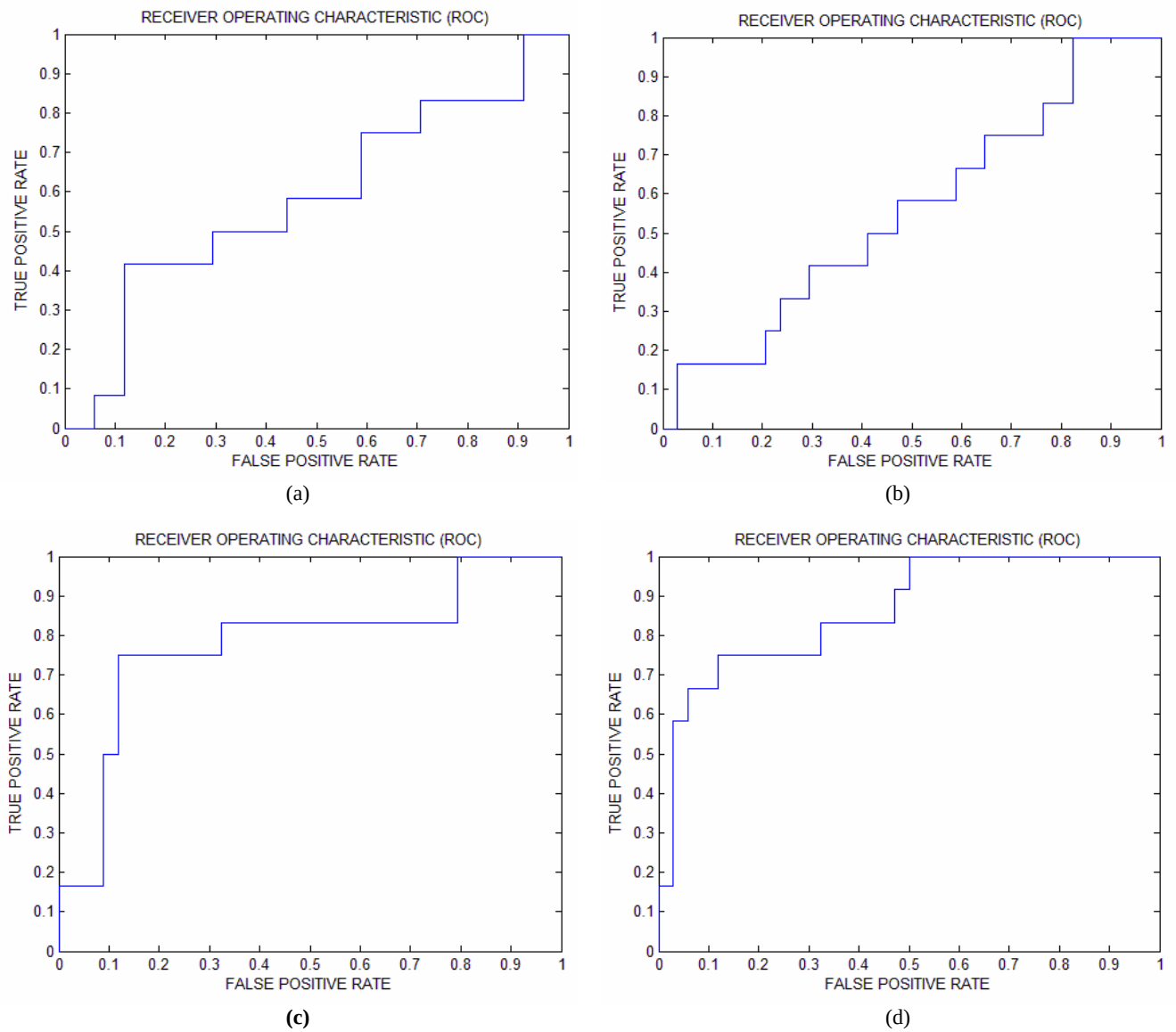

4.4 Discussion

In contrast to existing work on 2D skin line pattern features, this work has for the first time successfully utilised the 3D features, in the form of the 3D skin surface disruptions in surface normal data obtained from photometric stereo for the differentiation between MMs and benign lesions in vivo. Surface normal data belong to a form of illumination invariant 3D surface topographic texture, and reflect the microstructure information and inherent objectivity of 3D surfaces. They are in total contrast to the conventional 2D image texture used for deriving 2D skin line pattern features. This is because the 2D image texture inherently is the 2D image projection of 3D skin texture. It is not only subject to information loss as a result of the 3D to 2D projection but also subject to imaging noise such as specularities, shadows and other imaging errors during the projection. Therefore the proposed analysis of surface normals have the potential of providing a new, objective and more reliable approach for computer assisted diagnosis of MM.

5 Conclusions

This paper has proposed a new computer assisted system based on 3D skin surface normal features for diagnosing MM in vivo, which is an increasingly important medical subject. It is understood that diagnosing MM accurately is a very difficult task. However, based on the experimental results from this work, it has shown that by employing the proposed new 3D features, it can not only improve the understanding of the problem from a 3D perspective, but also substantially improve the accuracy of existing diagnosis based on the 2D skin line pattern features.

Acknowledgements

The authors would like to acknowledge the support of Department of Dermatology, Frenchay Hospital, Bristol (UK) and Royal Marsden NHS trust, Surrey (UK) for clinical trials using the skin analyser.

References

Bishop, C. (1995) *Neural networks for pattern recognition*, Oxford University Press.

Chetouani, Y. (2008) 'Using neural networks and statistical tests for detecting changes in the process dynamics', *International Journal of Modelling, Identification and Control (IJMIC)*, Vol. 3, No. 2, pp.113–123.

Ding, Y., Smith, L., Smith, M., Sun, J. and Warr, R. (2007) '3D skin texture analysis for early diagnosis for malignant melanoma', *Proceedings of Medical Image Understanding and Analysis*, pp.151–155.

Ding, Y., Smith, L., Smith, M., Sun, J. and Warr, R. (2008b) 'Enhancement of skin tilt pattern for lesion classification', *Proceedings of IASTED International Conference on Visualization, Imaging and Image Processing*, pp.1–6.

Ding, Y., Smith, L., Smith, M., Sun, J., Warr, R. (2008a) 'Obtaining 3D malignant melanoma indicators through the analysis of skin tilt pattern and skin slant pattern', *Proceedings of the MICCAI Workshop on Microscopic Image Analysis with Application in Biology (MIAAB)*, pp.64–71.

Duda, R., Hart, P. and Stork, D. (2001) *Pattern Classification*, 2nd eds., John Wiley & Sons.

Ercal, F., Chawla, A., Stoecker, W.V., Lee, H-C., Moss, R.H. (1994) 'Neural network diagnosis of malignant melanoma from color images', *IEEE Transactions on Biomedical Engineering*, Vol. 41, No. 9, pp.837–845.

Freeman J.A. and Skapura D.M. (1991) *Neural Networks: Algorithms, Applications and Programming Techniques*, Addison-Wesley.

Horn. B.K.P. (1986) *Robot Vision*, MIT press.

Karunakar, D.B. and Datta, G.L. (2008) 'Prediction of defects in castings using back propagation neural networks', *International Journal of Modelling, Identification and Control (IJMIC)*, Vol. 3, No. 2, pp.140–147.

Sboner, A., Eccher, C., Blanzieri, E., Bauer, P., Cristofolini M, Zumiani G. and Forti S.A. (2003) ,Multiple classifier system for early melanoma diagnosis', *Artif Intell Med*, Vol. 27, No. 1, pp.29–44.

She, Z., Liu, Y. and Damato, A. (2007) 'Combination of features from skin pattern and ABCD analysis for lesion classification', *Skin Research and Technology*, Vol. 13, No. 1, pp.25–33.

Smith, M.L, Farooq, A.R., Smith, L.N. and Midha, P.S. (2000) 'Surface texture inspection using conventional techniques applied to a photometrically acquired bump map', *Sensor Review*, Vol. 20, No. 4, pp.299–307.

Sun, J., Smith, M.L, Smith, L.N., Coutts, L., Dabis, R., Harland, C. and Bamber, J. (2008) 'Reflectance of human skin using colour photometric stereo: with particular application to pigmented lesion analysis', *Skin Research and Technology*, Vol. 14, No. 2, pp.173–179.

Sun, J., Smith, M.L., Smith, L.N., Midha, P.S. and Bamber, J. (2007) 'Object surface recovery using a multi-light photometric stereo technique for non-Lambertian surfaces subject to shadows and specularities', *Image and Vision Computing*, Vol. 25, pp.1050–1057.

Weickert, J. (1998) Anisotropic Diffusion in Image Processing, Teubner.